Journal of Structural Geology 30 (2008) 1192–1200

Contents lists available at ScienceDirect

Journal of Structural Geology

journal homepage: www.elsevier.com/locate/jsg

The control of salt supply on entrainment of an anhydrite layer within a salt diapir

Zurab Chemia*, Hemin Koyi

Hans Ramberg Tectonic Laboratory, Solid Earth Geology, Department of Earth Sciences, Uppsala University, SE-752 36 Uppsala, Sweden

ARTICLE INFO

Article history:
Received 6 November 2007
Received in revised form 22 May 2008
Accepted 10 June 2008
Available online 17 June 2008

Keywords:
Salt supply
Anhydrite
Numerical modelling
Sinking
Entrainment

ABSTRACT

The influence of four parameters (sedimentation rate, viscosity of salt, stratigraphic location of the anhydrite layer within the salt layer, and the perturbation width) on salt supply to down-built diapirs and its entrainment capacity are studied systematically in numerical models. Model results show that these four parameters affect salt supply, and the evolution history of a salt diapir. As such, these parameters strongly influence the style and the amount of entrainment of dense inclusions into a diapir. In active diapirs (i.e. unburied diapirs), salt supply increases with increasing sedimentation rate whereas it decreases with an increase in salt viscosity. Diapirs initiating from wide perturbation provide more salt supply to feed the diapir. Presence and initial stratigraphic location of any denser layer (e.g. an anhydrite layer) within a salt layer also affects salt supply. When lateral forces are negligible, salt supply into a diapir depends on these four parameters, which directly control the entrainment of any embedded anhydrite layer into the diapir.

1. Introduction

Salt in structures like pillows and diapirs are common features in many sedimentary basins (e.g. Jenyon, 1986). These structures form from initially sub horizontal or slightly inclined layers. Salt structures are defined as tectonically active when they rise due to differential loading created by the overburden layers and/or by regional tectonics (Koyi, 1988; Jackson et al., 1994; Koyi, 1998; Hudec and Jackson, 2007). A diapir may become inactive (and stops rising) when the driving forces (differential loading, regional tectonics) cease, the source layer is depleted or a strong lid covers the diapir and prevents it from further rise.

The geometry of an active diapir is moulded by six parameters: rate of salt supply, dissolution, sediment accumulation, erosion, extension, and shortening (Koyi, 1998). The rate of salt supply is the rate at which salt flows from the source layer into the diapir and contributes to its growth. In a system where lateral movement (extension and shortening) is insignificant, salt supply and sedimentation rate govern the evolution of a down-built diapir (Vendeville et al., 1993; Koyi, 1998). If the rate of salt supply is less than the rate of sediment accumulation, upward-narrowing diapirs form. In contrast, upward-widening diapirs form when the salt supply is greater than the rate of sediment accumulation and columnar diapirs form when the rate of salt supply is equal to the rate of sediment accumulation (Jackson and Talbot, 1991; Vendeville and Jackson, 1993; Vendeville et al., 1993; Jackson et al., 1994; Talbot, 1995; Koyi, 1998).

Inclusions of denser rocks are common in salt diapirs. The size and lithology of such entrained inclusions varies from place to place. Sedimentary, volcanic and even some plutonic inclusions (several kilometres in diameter) characterize many of the diapirs in the Zagros fold-thrust belt (Kent, 1979). Many of the inclusions are related to the original salt deposits or are older (Gansser, 1992). On Hormuz island, inclusions of white rhyolites and trachytes frequently occur as irregular masses up to 1 km long while a few are more plug-like (Gansser, 1992). Many salt diapirs contain varying amounts of other evaporite rocks, especially anhydrite or its hydrated form, gypsum, and/or non-evaporite rocks. Most non-halite inclusions in salt are originally interbedded with the salt (e.g. Zechstein formation). The Gorleben salt diapir in Germany carried large blocks of an anhydrite. The internal structure of the Gorleben diapir includes vertical or steeply inclined fold axes (Zirngast, 1996). The Main Anhydrite from the Gorleben diapir is a very important layer with respect to nuclear waste storage (Bauerle et al., 2000; Koyi, 2001).

Analogue and numerical models confirm that denser block can be entrained by diapiric flow if the rate of diapiric rise is greater than rate of decent of the denser entrained blocks (Weinberg, 1993; Koyi, 2001; Chemia et al., 2008). The results of numerical models have shown that most power-low salt diapirs would be capable of lifting inclusions up to 3–6 km^2 (a horizontal cross-sectional area) if

* Corresponding author. Fax: +46 18 471 2591.
E-mail address: zurab.chemia@geo.uu.se (Z. Chemia).

0191-8141/$ – see front matter © 2008 Elsevier Ltd. All rights reserved.
doi:10.1016/j.jsg.2008.06.004

these rise at geological reasonable velocities (Weinberg, 1993). Analogue and numerical models carried out by Cruden et al. (1995) investigating the entrainment of high density and high viscosity materials into buoyant diapirs predict the entrainment of a denser layer. In models used by Cruden et al., where the dense layer was situated directly on a rigid basement beneath the buoyant layer, the amount of the denser layer that was entrained varied as a function of the ratio of the density contrasts between the layers, the viscosity ratio, and relative thicknesses of the layers.

In an earlier paper the parameters that influence entrainment of an anhydrite layer, originally embedded within the salt layer, into Newtonian salt diapir was studied (Chemia et al., 2008). The results showed that the ability of salt to entrain anhydrite blocks depends on (i) sedimentation rate, (ii) viscosity of salt, (iii) perturbation width and (iv) initial stratigraphic location of the embedded anhydrite layer. In this current study, we investigate in detail the influence of these four parameters on salt supply during the development of a diapir down-built from a salt layer with an initially intercalated denser anhydrite layer. Using two-dimensional numerical calculations, a whole range of values for these four parameters are explored. To investigate the entrainment of a denser layer, which depends on multiple parameters, we combine these parameters into a single parameter, which is the rate of salt supply (volume/area of the salt that is supplied to the diapir with time, i.e. cumulative flow of salt from the salt layer to the diapir). In the following sections, we will show how sedimentation rate, viscosity of the salt, stratigraphic location of the denser layer and width of the perturbation influence salt supply.

2. Numerical concept

This study is based on numerical models deployed to simulate the dynamics of multi-compositional salt tectonics (Chemia et al., 2008). The governing equations describing dynamic evolution are solved by finite differences (FD) on an equidistant grid in a rectangular box of aspect ratio = 1. The markers technique is used to model multi-compositional flows where each composition has a different rheological property and density. The deformation behaviour of the rock is described by power-law ductile creep (Kirby and Kronenberg, 1987). Where viscosity is related to nth power of deviatoric stress, which is given as:

$$\eta = A\tau_{\mathrm{II}}^{1-n} \quad (1)$$

where A is a pre-exponential constant, and τ_{II} is the 2nd invariant of the stress tensor. A full description of the mathematical formulation and its numerical implementation are given in Weinberg and Schmeling (1992) and Chemia et al. (2008).

The models presented here loosely simulate the Gorleben diapir. Therefore, the model dimension (4 × 4 km) is chosen to be similar to the Gorleben diapir with a no-slip bottom boundary, a free-slip top boundary, and reflective lateral boundaries (Fig. 1). In all model runs, the salt layer simulating the 1040-m thick Zechstein formation (e.g. Zirngast, 1996) rests initially at the base of the model (Fig. 1). An anhydrite layer is modelled as an 80-m thick layer embedded within the Zechstein salt formation. A 160-m thick pre-kinematic layer of overburden is placed on the top of the salt layer leaving a wide gap to act as a perturbation (P_w), which triggers the diapir. Then the diapir is down-build by sedimentary units. Sediments accumulate as horizontal layers that thicken the overburden at a given constant rate, $\dot{s}_e$. The initial position of the sediment surface is given by the top of the pre-kinematic overburden, which is the same in all models (h_3 = 160 m). If the salt surface lies below newly deposited sediments, then the salt is also covered with sediments. Numerical models do not include the effects of salt loss by dissolution or sediment compaction.

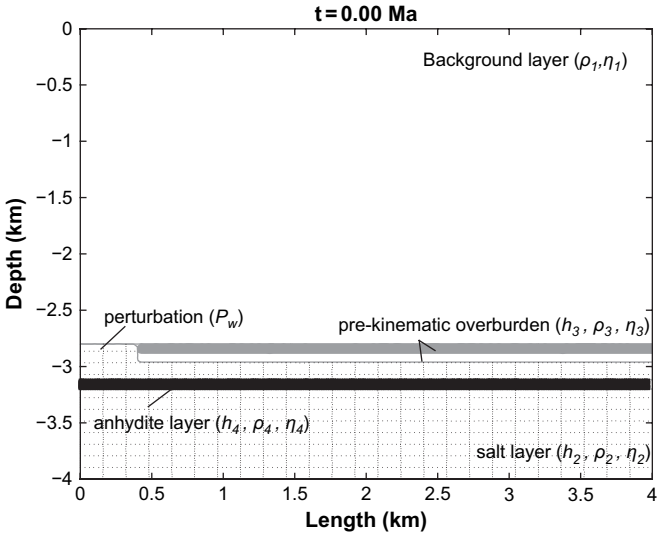

Fig. 1. Initial condition and parameters used in the models. The box has no-slip at the bottom, free-slip at the top and reflective side boundaries. The box can be considered as showing the right hand half of a symmetric structure.

3. Material properties

In situ salt properties can be approximated by Newtonian-viscous rheology (Baar, 1977; Jackson and Talbot, 1986). In most modeling studies, an average salt viscosity of 10^{17}–10^{18} Pa s is used (Urai et al., 1986; Spiers et al., 1990; Carter et al., 1993; Van Keken et al., 1993). However, the deformation mechanism for salt is temperature and grain size dependent. The effective viscosity of salt ranges from 10^{17} Pa s for small grain size and high-temperature salt to l0^{20} Pa s for large grain size and low temperature salt (Van Keken et al., 1993). We model salt with Newtonian-viscous rheology and a range of effective viscosities (10^{17}–10^{19} Pa s). A mean value of the density for rock salt is assumed to be 2200 kg m^{-3} (Landolt-Boernstein, 1982).

In the models presented in this paper, it is supposed that the overburden rocks behave as non-Newtonian materials or as brittle solids. The sedimentary units (overburden rocks), in all our models are simulated with higher viscosity (effective viscosity ranges between 10^{23}–10^{25} Pa s, n = 4) instead of a Newtonian rheology previously used in analogue and numerical modelling (e.g. Biot, 1965; Ramberg, 1968; Woidt, 1978; Poliakov et al., 1993). The purpose of using high viscosity overburden, which simulates sedimentary units within the upper crust, is to avoid deformation of the upper crustal rocks by viscous flow. In this study, we focus on the internal deformation of a diapir with the assumption that the overburden, similar to natural cases, does not deform viscously. Our assumption of a very high viscosity keeps viscous behaviour in the overburden extremely small.

The anhydrite layer is assigned power law rheology (n = 2) independent of temperature (Kirby and Kronenberg, 1987). Since the modelling approach is based on the mechanics of continua rather than fracture mechanics, the brittle rheology of anhydrite cannot be achieved in numerical models. However, there are ample geological observations, which show that anhydrite behaves as incompetent material (Van Berkel et al., 1986; Heilbronner and Bruhn, 1998; Behlau and Mingerzahn, 2001). We model anhydrite with an effective viscosity ranging between 10^{19}–10^{21} Pa s, higher than the viscosity of salt.

4. Model calculations

Numerical runs are carried out so that one of the four parameters [sedimentation rate ($\dot{s}_e$), width of the initial perturbation (P_w), salt viscosity (η_2), and stratigraphic location of the anhydrite layer (L_a)] is varied systematically where the others are kept constant. The density and viscosity of the background material (ρ_1, η_1), sedimentary layers (ρ_3, η_3), and the anhydrite layer (ρ_4, η_4) are kept constant in all sets of experiments (Table 1). After initiation, the diapir is down-built to a height of 3.6 km. A 400-m thick, stiff overburden layer is placed on the top of the diapir, which stops its further growth. Covering the diapir with a thick and stiff overburden simulates post diapiric state when the diapir is externally inactive.

At different stages of the diapir growth, the area of the diapir and the area of the entrained anhydrite layer are calculated. The area of the diapir is defined by the contour comprising the chemical composition of the salt layer. The contour is closed at the level of the perturbation, which might sink or rise during the model evolution and the area is calculated above this dynamic level (Fig. 2). Similarly, we define that the anhydrite is entrained if it is carried upward into the diapir above the perturbation level. The amount of the entrained anhydrite layer is defined by the closed contour comprising the chemical composition of the anhydrite layer above the perturbation level (Fig. 2). If the anhydrite layer is disrupted then the cumulative area of the entrained anhydrite is considered the sum of the areas of the closed contours above the perturbation level (Fig. 2).

In the two dimensional numerical experiments, the parameter cumulative percentage entrainment (E) is conveniently defined as $E = (A_t/A_0) \times 100$, where A_t is the area of anhydrite layer which has moved above a reference line (set at the perturbation level) at any given time (t) and A_0 is the original area of the anhydrite layer at $t = 0$ (Fig. 2). Similarly, cumulative percentage salt supply (S) is defined as $S = (A_t/A_0) \times 100$, where A_t is the area of salt layer which has moved above a reference line (area of the diapir, Fig. 2) at any given time (t) and A_0 is the original area of the salt layer beneath the surface at $t = 0$ (Fig. 2).

5. Results

The results presented in this paper are based on models which are described in Chemia et al. (2008). In this article, we extend the range of the parameters and recast results in terms of salt supply. We use model results to highlight the effect of four parameters on rate of salt supply, which in turn governs the mode and rate of anhydrite entrainment.

5.1. Sedimentation rate

Several models are deployed to investigate how salt supply to a diapir is influenced by sedimentation rate (i.e. the rate at which the diapir is down-built). The viscosity of salt in these models is fixed at 10^{17} Pa s, the width of the perturbation to 400 m and the anhydrite layer is placed within the upper half of the salt layer. In these models, sedimentation rate varies from 5 to 0.05 mm a^{-1}.

Table 1
Model parameters

Quantity	Symbol	Value
Domain height		4000 m
Domain width		4000 m
Density of the background	ρ_1	1000 kg/m^3
Viscosity of the background	η_1	10^{16} Pa s
Density of the salt	ρ_2	2200 kg/m^3
Viscosity of the salt	η_2	10^{17}–10^{19} Pa s
Thickness of the salt	h_2	1040 m
Density of the overburden	ρ_3	2600 kg/m^3
Viscosity of the overburden	η_3	10^{23}–10^{25} Pa s; $n = 4$
Thickness of the pre-kinematic layer	h_3	160 m
Density of the anhydrite	ρ_4	2900 kg/m^3
Viscosity of the anhydrite	η_4	10^{19}–10^{21} Pa s; $n = 2$
Thickness of the anhydrite	h_4	80 m

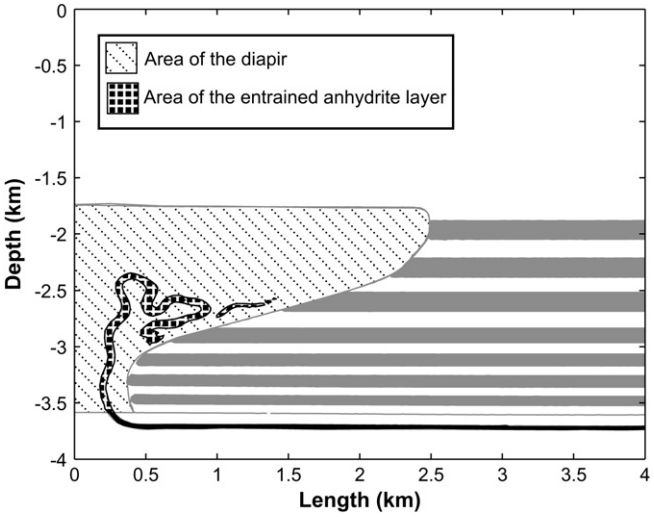

Fig. 2. Illustrated areas of the diapir and the entrained anhydrite layer used for calculated salt supply and entrainment.

As expected, variation in sedimentation rate results in diapirs with different shapes. In models where rate of sedimentation ($\dot{s}_e = 5$ and 4 mm a^{-1}) exceeds the rise rate of the diapir sediments bury the perturbation in the early stages of its evolution and the salt remains static in the subsurface for several million years. In these models the driving force provided by aggrading sediments at a constant rate (5 and 4 mm a^{-1}) is not sufficient to overcome the strength of the encasing sediments. When the sediments bury the initial perturbation, salt supply is zero and the denser anhydrite layer initially embedded within the salt layer starts to sink due to its negative buoyancy.

In models with slower sedimentation rate (3–0.5 mm a^{-1}), salt flows into the diapir and develops overhangs ranging in width from 0.92 to 3.06 km. In these models, the crest of the diapir remains uncovered (salt flow velocity into the diapir is faster than the sedimentation rate) and the anhydrite layer is entrained by the diapirs to different levels (Figs. 3 and 4B). As long as the diapir is not buried, salt supply to the diapir in these models increases with increasing sedimentation rate (Fig. 4A).

In models where the sedimentation rate is very slow (0.25–0.05 mm a^{-1}), an upward widening diapir forms, that produces a wide overhang. Segments of the anhydrite layer are entrained into the diapir and displaced sideways into the overhang. The pre-kinematic overburden bends towards the diapir, sinks and cuts the supply of salt to the diapir. Continued sedimentation over the crest of the diapir in these models forms sinking mini-basins. Overburden units in the mini-basins deform as they sink into the diapir overhang and segment it. Entrained anhydrite segments are displaced by these sinking mini-basins. In these models, salt supply into the diapir decreases with decreasing sedimentation rate (Fig. 4). The formation of diapir with complicated geometries (segmented into mini-basins) restrains entrainment of the intercalated anhydrite layer in places of slow vertical salt flow.

5.2. Viscosity of salt

Modeling more viscous salt ($\eta_2 = 5 \times 10^{17}$ Pa s) requires a decrease in the sedimentation rate significantly since even 1 mm a^{-1} sedimentation rate exceeds the rate of diapir rise and the diapir is

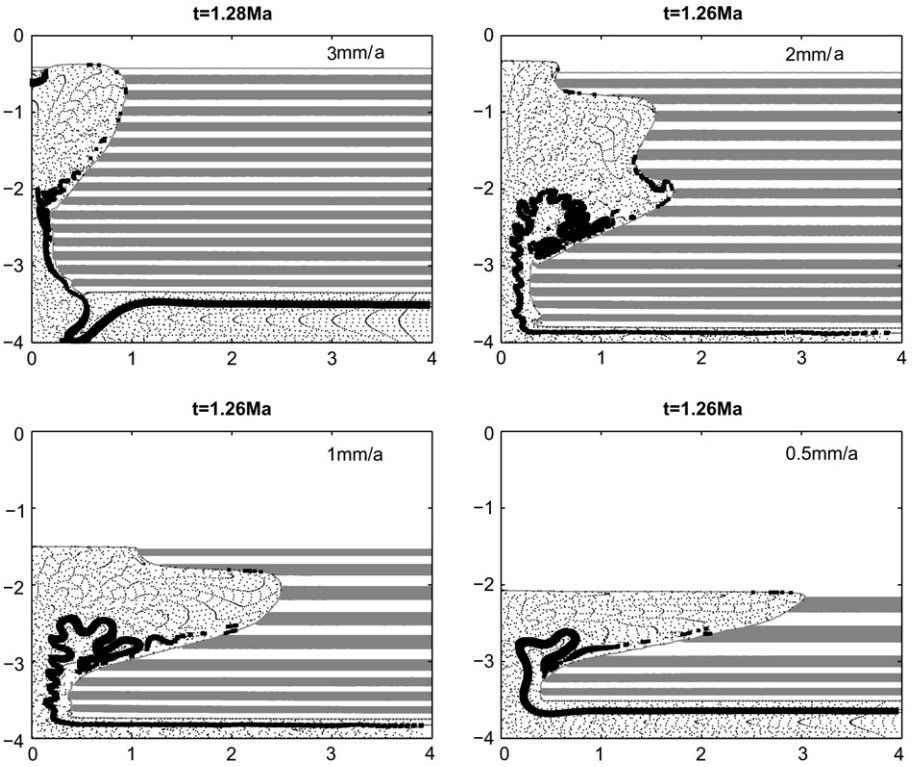

Fig. 3. Snapshots of four models with different sedimentation rates (3, 2, 1 and 0.5 mm a^{-1}) showing the development of diapirs and the entrained anhydrite layer. The viscosity of the salt, the initial width of the perturbation and stratigraphic location of the anhydrite is the same in these models ($\eta_2 = 10^{17}$ Pa s, $P_a = 400$ m and $L_a = 800$ m, respectively).

buried. Therefore, models that target variation of viscosity of salt are performed with slow sedimentation rates (0.1 and 0.05 mm a^{-1}) to allow a diapir to form. Increasing salt viscosity changes the shape of the diapir through changing its salt supply. Increasing salt viscosity for a particular constant sedimentation rate significantly decreases salt supply and the entrainment of the anhydrite layer (Fig. 5). Increase of viscosity by an order of magnitude and decrease of sedimentation rate by the same order often result in diapirs of similar geometries. The shape of the diapir becomes columnar-like when the rate of sedimentation is close to the rate of salt supply. However, if the salt is given such a viscosity that the sedimentation rate exceeds the rate of salt supply (e.g. model with salt viscosity 10^{19} Pa s and sedimentation rate 0.1 mm a^{-1}), the diapir starts to narrow upward and it is finally buried by the

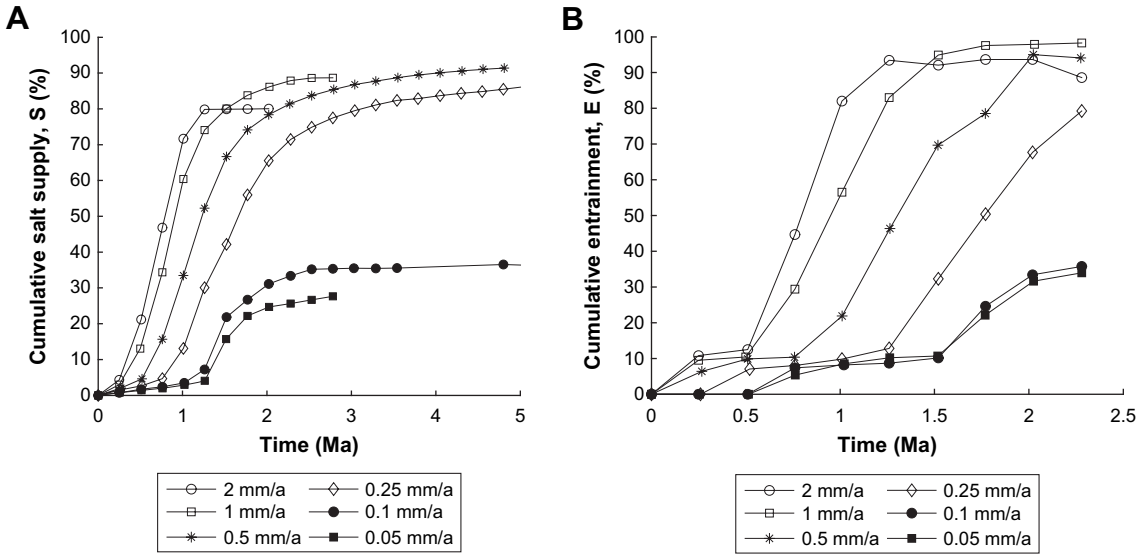

Fig. 4. (A) Effect of the sedimentation rate on salt supply. (B) The cumulative percentage entrainment (E) of an anhydrite layer in models with different sedimentation rates (2–0.05 mm a^{-1}). Plots show change in cumulative percentage salt supply (S) and cumulative percentage entrainment (E) with time in models where only the sedimentation rate is varied (2–0.05 mm a^{-1}). The viscosity of the salt, the initial perturbation width and the stratigraphic location of the anhydrite layer are kept the same ($\eta_2 = 10^{17}$ Pa s, $P_w = 400$ m and $L_a = 800$ m, respectively). Salt supply is plotted until the diapir is covered by a stiff overburden layer (sedimentation rates 2, 1 and 0.5 mm a^{-1}) or the diapir is strongly segmented into mini-basins (sedimentation rates 0.25, 0.1 and 0.05 mm a^{-1}). Models with sedimentation rates 5 and 4 mm a^{-1} are not shown here because they are buried in the early stages, thus, salt supply is zero.

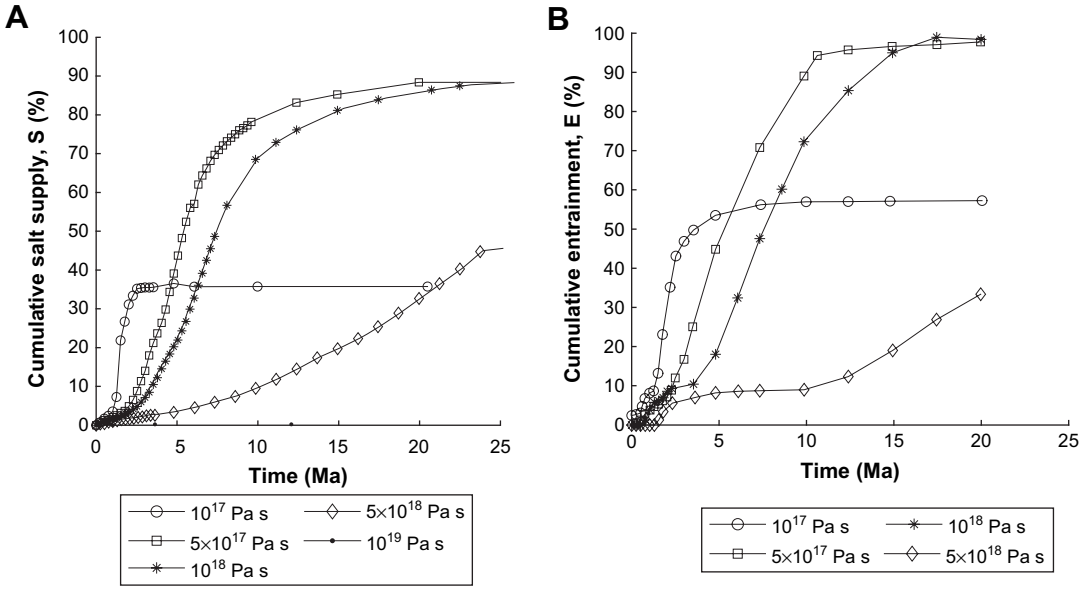

Fig. 5. (A) Effect of the salt viscosity on cumulative salt supply. Plot shows the area of the diapir in percentage for the diapirs formed with different salt viscosities ($\eta_2 = 10^{17}$–10^{19} Pa s) and the same sedimentation rate (0.1 mm a^{-1}), perturbation width (800 m), and the stratigraphic location of the anhydrite layer (800 m). The diapir with salt viscosity 10^{19} Pa s and sedimentation rate 0.1 mm a^{-1} is buried in the early stages. (B) The cumulative percentage entrainment of the anhydrite layer for the same models where only salt viscosity is varied.

accumulated sediments on its crest. The entrainment in these models continues until the supply of salt ceases or the diapir is buried.

5.3. Stratigraphy of the source layer

Several models are run where only the initial stratigraphic location of the anhydrite layer is changed. Since rapid sedimentation would bury a potential diapir, we chose a slow sedimentation rate (0.1 mm a^{-1}) to investigate the influence of the stratigraphy of the source layer on the evolution of the diapir, its salt supply, and entrainment of the anhydrite layer. Salt is assigned viscosity 5×10^{17} Pa s and a diapir is triggered from a 400-m wide rectangular perturbation.

In these models, diapirs first evolve into a column of salt and then widen upward by increasing withdrawal of salt from the source layer. When the anhydrite layer is located in the upper half of the salt layer, salt initially is supplied into the stem of the diapir from the upper thinner salt sequence. However, the thin upper salt sequence does not provide sufficient salt flow. Instead, salt starts to flow from the lower salt sequence where the anhydrite layer acts as a lid (Fig. 6A). As a result, salt from the lower sequence pushes the anhydrite layer and bends it upwards. In contrast, in a model where the anhydrite is located in the lower part of the source layer, salt flow is dominated by flow from the upper thicker salt sequence (Fig. 6C). On the other hand, salt flow equally distributes in the models where the anhydrite layer is located in the middle of the source layer (Fig. 6B).

Regardless of different stratigraphic location of the anhydrite layer (which induces salt flow within different parts of the source layer), the crest, or height of the diapir evolves with negligible difference (Fig. 6). However, these diapirs differ in the width of their overhang and the style of the anhydrite entrainment. After 6 Ma, a wider overhang (3 km) forms in the model where the anhydrite layer is located in the upper half of the salt layer, whereas in the model where the anhydrite layer is located in the lower half, a relatively narrower overhang (2.6 km) formed. The model where the anhydrite layer is located in the middle of the salt layer develops smallest overhang and shows intensive folding of the embedded anhydrite layer relative to models where the anhydrite layer is located in the upper or lower half of the source layer. The anhydrite layer folds strongly during its rise and fall (Fig. 6B).

5.4. Perturbation width

A set of models are deployed to investigate the influence of the perturbation width on salt supply. In this section, we present models where the anhydrite layer is located in the upper half of the source layer (L_a = 800 m), sedimentation rate is 1 mm a^{-1}, viscosity of salt $\eta_2 = 10^{17}$ Pa s, whereas perturbation width is changed (400, 800, 1200 and 1600 m).

In models with high sedimentation rates (4 and 5 mm a^{-1}) and viscosity ($\eta_2 = 10^{17}$ Pa s) an increase of perturbation width from P_w = 400 m to P_w = 800 m still does not induce sufficient salt flow which could overcome the fast rate of sedimentation. The perturbation is then buried in the early stages of the model evolution. However, the effect of increased perturbation width is shown in models where the sedimentation rate does not bury the initial perturbation ($\dot{s}_e$ = 3–0.1 mm a^{-1}).

An 800-m wide perturbation initiates rapid salt flow in the model where $\dot{s}_e$ = 1 mm a^{-1} and $\eta_2 = 10^{17}$ Pa s. The diapir rises with similar rate to sedimentation rate and forms columnar stem in the early stages of the evolution. At later stages, the feeding stem becomes wider due to increased salt supply. Hence, fast withdrawal of salt pulls the anhydrite layer from the source into the perturbation, where viscous drag carries it upward. The substantial withdrawal of the salt results in thinning of the source layer and a decrease in salt supply. In the very later stages, the diapir starts to narrow upward. A 400 m thick stiff layer of the overburden, which is placed on the top of the diapir, prevents it from further rise and the early-entrained anhydrite layer starts to descend due to the lack of the salt supply (Fig. 7).

A similar model evolution is observed by increasing perturbation width to 1200 m. Salt supply to the diapir increases with increase in width of the initial perturbation (Fig. 7A).

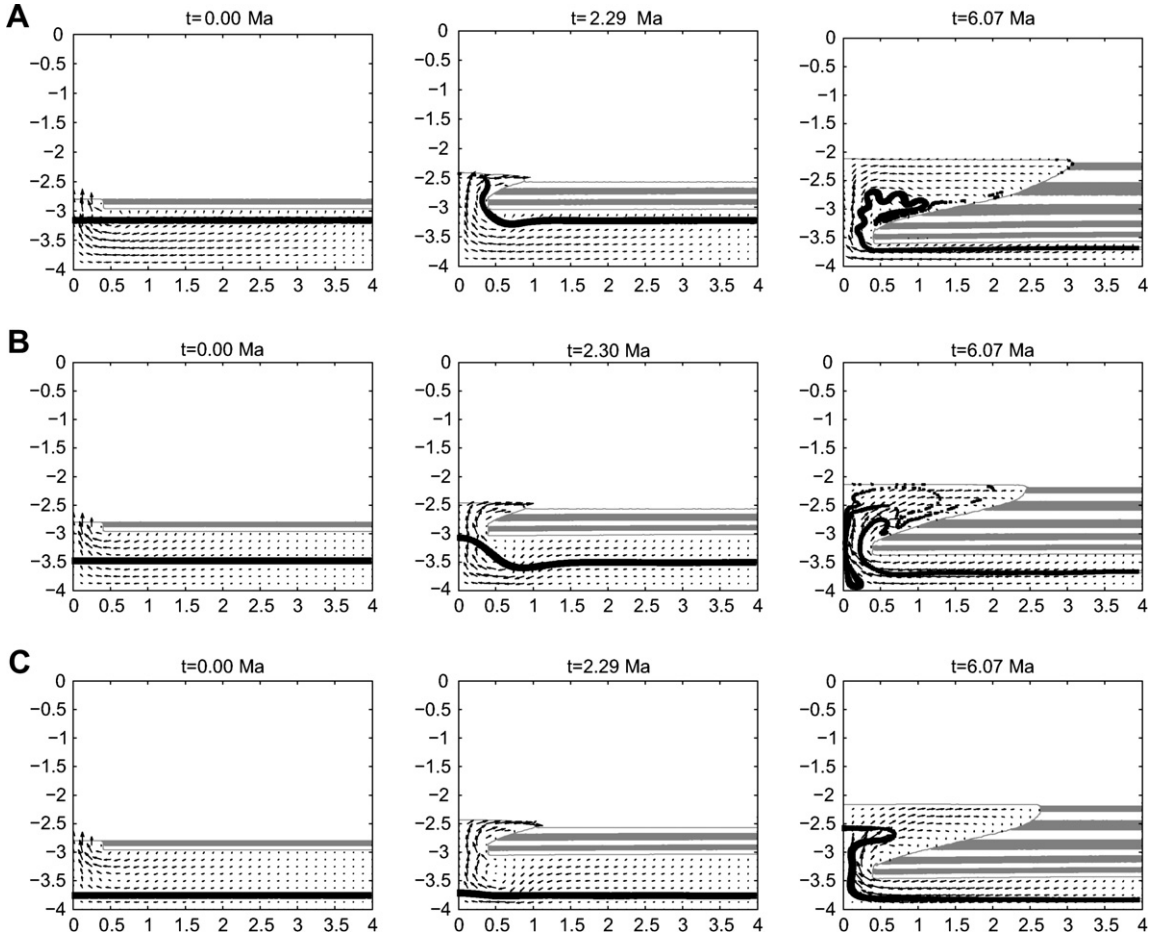

Fig. 6. Snapshots of the evolution of the diapirs in models with varied stratigraphy of the anhydrite layer. The anhydrite layer is located; (A) in the upper half of the source layer, $L_a = 800$ m, (B) in the middle of the source layer, $L_a = 480$ m, and (C) in the lower part of the source layer, $L_a = 200$ m. Model parameters are identical except stratigraphy of the source layer. Sedimentation rate is 0.1 mm a^{-1}, viscosity of salt is 5×10^{17} Pa s and perturbation width is 400 m.

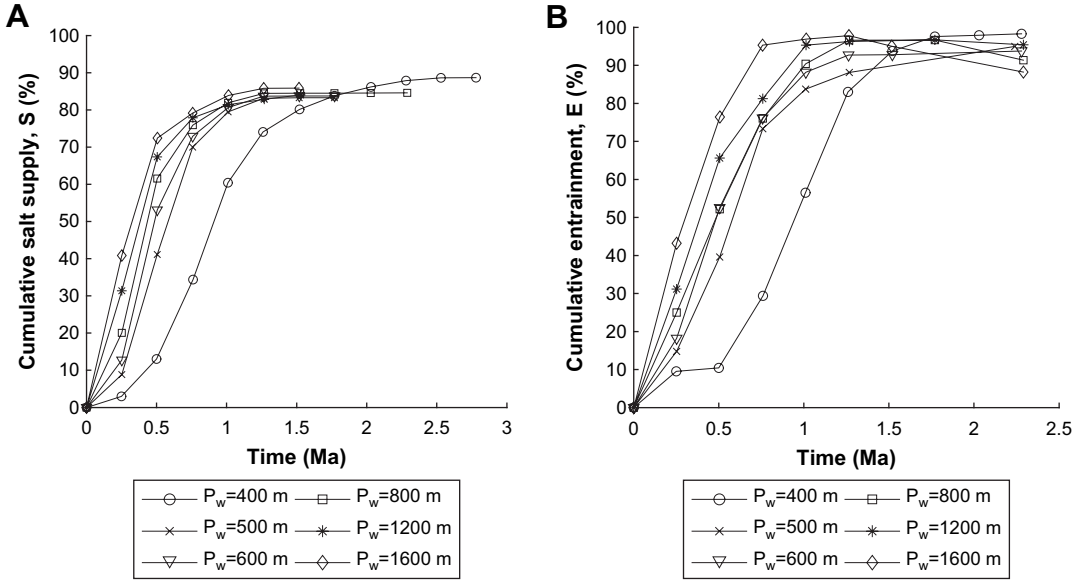

Fig. 7. (A) Effect of the perturbation width on cumulative salt supply in models where only perturbation width varies. (B) Cumulative entrainment of the anhydrite layer. Model parameters are: sedimentation rate, $\dot{s}_e = 1$ mm a^{-1}, salt viscosity, $\eta_2 = 10^{17}$ Pa s, stratigraphic location of the anhydrite layer, $L_a = 800$ m and the width of the perturbation varies from 400 to 1600 m.

6. Discussion

Depending on the evolution history of model diapirs, keeping viscosity constant at $\eta_2 = 10^{17}$ Pa s and perturbation width $P_W = 400$ m we distinguish three ranges of sedimentation rate. (I) High sedimentation rates (5 and 4 mm a^{-1}), which bury the initial perturbation and results in an immediate sinking of the embedded anhydrite layer within the salt layer. In this case, salt supply to the perturbation is zero and the anhydrite layer is not entrained. (II) Intermediate sedimentation rates (3–0.5 mm a^{-1}) that are initially less than the rate at which the crest of the diapir is growing so that the crest of the diapir remains uncovered and provides highest salt supply. Models with intermediate sedimentation rate are characterized by high percentage entrainment (80–90%, Fig. 4B). (III) Slow sedimentation rates (0.25–0.05 mm a^{-1}) that segments the diapir due to formation of mini-basins, reduces salt supply. Entrainment of the anhydrite layer in these models is limited (less than 30%, Fig. 4B).

Although the viscosity of salt significantly alters salt supply, the down-build diapirs grow in height at essentially similar rates. The variation in salt supply results in the formation of overhangs of different width. However, the effect of the viscosity variation on rate of rise of the crest of the diapir is negligible (Chemia et al., 2008).

Comparison of models where only the viscosity of the salt varies for a fixed sedimentation rate (0.1 mm a^{-1}) shows that salt supply increases with decrease in salt viscosity (Fig. 5A). A faster flowing low viscosity salt ($\eta_2 = 5 \times 10^{17}$ Pa s) entrains higher amount (80–90%) of the anhydrite at a faster rate than a slower flowing high viscosity salt ($\eta_2 = 5 \times 10^{18}$ Pa s, entrainment does not exceed 10% in 10 Ma, Fig. 5B). The fast entrainment rate in model with salt viscosity $\eta_2 = 10^{17}$ Pa s can be retarded if the diapir is segmented and salt supply is cut by the bending pre-kinematic layer. Even though the viscous drag along the boundaries of the anhydrite blocks is higher in models with high viscosity salt, more viscous salt flows slower than a less viscous salt (with the same sedimentation rate and thus the same differential loading) the overall entrainment is more effective within low viscosity salt.

The stratigraphic position of the anhydrite layer influences salt flow within the diapir, which can be seen by comparing the cumulative area of the diapir. The fastest growing diapir is where the anhydrite layer is absent (Fig. 8A). Model diapirs with an embedded anhydrite layer grow slower because their salt supply is retarded compared with a salt layer without an anhydrite layer. In addition, in models where the anhydrite layer is embedded within the salt layer the stratigraphic location of the anhydrite layer influences the rate of salt supply into the diapir with time. Salt supply is proportional to thickness of salt layer. Thus, when the anhydrite layer is embedded within the salt it splits the source layer into two layers where each of the layers flows with different rate. Flow is highest where the salt is thicker. Intuitively one could think of most efficient entrainment when the fast salt flow is below the anhydrite layer. Viscous drag acting on an anhydrite layer located in the upper part of the salt layer is less than in models where the anhydrite layer is located in the middle of the salt layer (Fig. 8A). Therefore, most entrainment occurs in models where the anhydrite layer is located in the middle of the salt layer (Fig. 8B). The drop in salt supply causes the anhydrite layer, which is entrained and transported into the overhang in early stages, to sink back into the diapir.

The rate of thinning of the source layer confirms that when the anhydrite layer is in the lower part of the salt sequence, most of the salt is withdrawn from the initially thicker upper sequence of the salt layer (Fig. 9). The same is true for the lower part of the salt layer when the anhydrite layer is embedded in the upper half of the salt sequence (Fig. 9C). Comparison of the rate of the thinning of the salt layers for models with different stratigraphic position of the anhydrite layer and the model where the anhydrite layer is missing shows that flow within the salt layer is sensitive to the stratigraphic position of the anhydrite layer as well as thickness change of the source layer (Fig. 9). If the anhydrite layer is located in the middle of the salt sequence then the upper and the lower parts of the salt layer thin at the same rate, this approaches the same rate as in the model without an anhydrite layer (Fig. 9B).

The set of models where only the perturbation width varies shows that width of the perturbation alters the geometry of the diapir through influencing the rate of salt supply and hence the degree of anhydrite entrainment. Wide perturbations supply significantly larger volumes of salt into the diapir so that the source layer in such models depletes much faster. Consequently, diapirs triggered with initially wide perturbation grow fast. The viscous drag within the stem is higher in models where the perturbation is initially wide, therefore, the anhydrite layer is entrained more effective in models where the perturbation is wider and salt supply

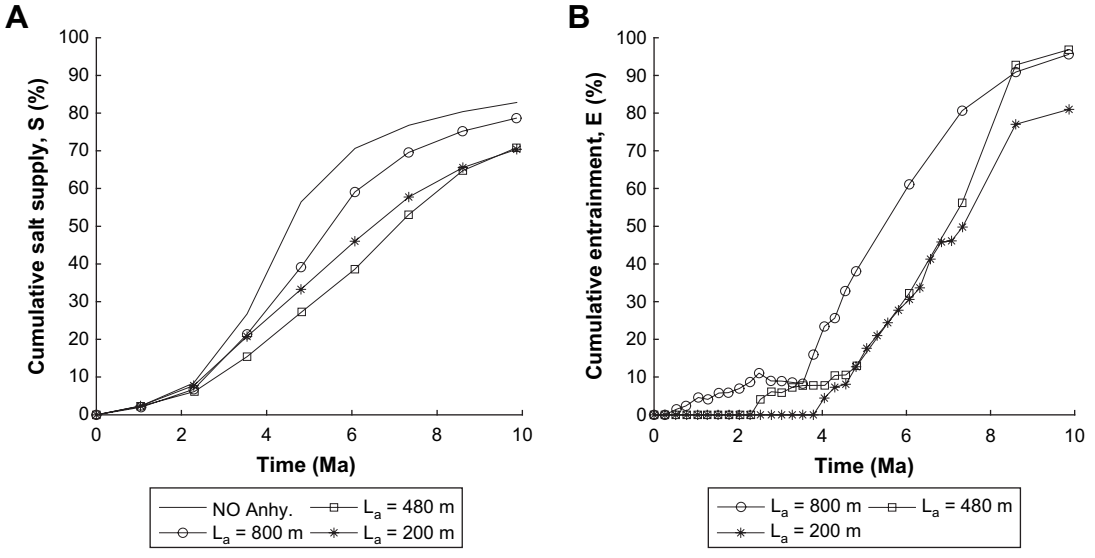

Fig. 8. (A) Effect of the stratigraphic location of the anhydrite layer on cumulative salt supply. Plot shows the area of the diapir in percentage for the diapirs formed with different stratigraphic location of the anhydrite layer. The viscosity of the salt, the initial perturbation width and the sedimentation rate are kept the same ($\eta_2 = 5 \times 10^{17}$ Pa s, $P_w = 400$ m and $\dot{s}_e = 0.1$ mm a^{-1}, respectively). (B) The cumulative percentage entrainment of the anhydrite layer.

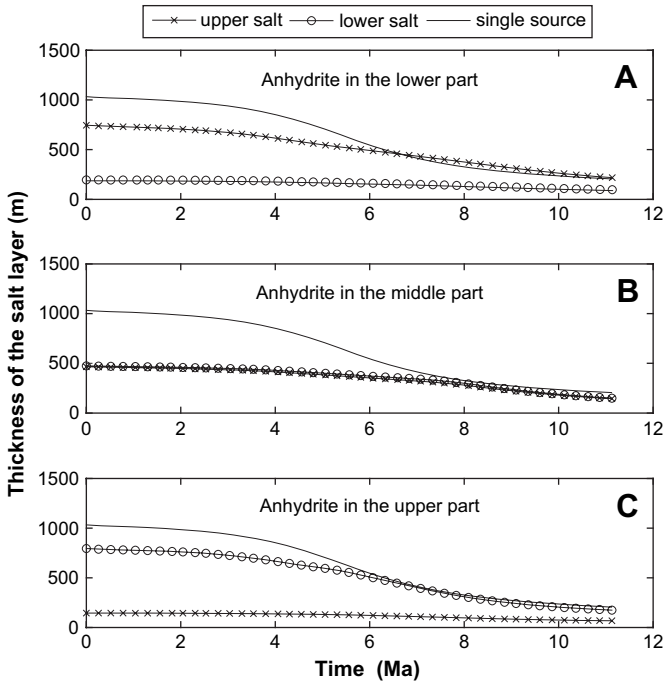

Fig. 9. Plot of the thickness of the upper and lower salt layers during the evolution of the models where the stratigraphic position of the anhydrite layer is varied. The anhydrite layer is located; (A) in the lower part of the salt layer, (B) in the middle part of the salt layer, and (C) in the upper part of the salt layer. These models differ only in stratigraphy of the salt layer whereas sedimentation is 0.1 mm a^{-1}, salt is given viscosity of $\eta_2 = 5 \times 10^{17}$ Pa s and the perturbation width is 800 m. We present the thickness of the salt layer at the margin, away from the diapir. This thickness is the maximum thickness of the salt layer in the case of segmented diapirs. However, if the diapir is actively growing since the overburden unit does not deform the thickness of the salt layer beneath the overburden is uniform.

is greatest (Fig. 7A,B). The effect of the increased initial perturbation width on salt supply is high in models where it is 800 m.

Variation in sedimentation rate moulds diapirs into different geometries varied from upward narrowing to upward widening and columnar as well as very complex geometries (segmented diapirs). The height of the down-built diapirs where only the sedimentation rate is varied evolves proportionally to the sedimentation rate. An increase in sedimentation rate increases the rate at which the crest of the diapir rises (Fig. 10).

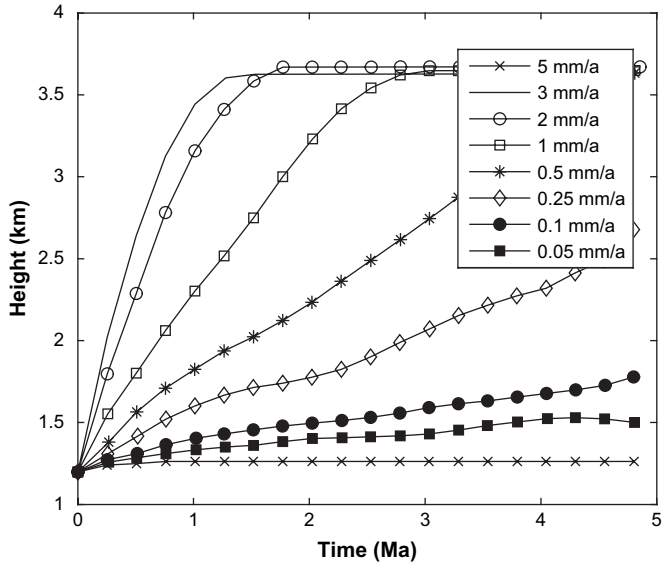

Fig. 10. The evolution of the crest of the diapir in models with different sedimentation rates (5–0.05 mm a^{-1}). In all these models, the viscosity of the salt, the initial perturbation width and the stratigraphic location of the anhydrite layer are kept the same ($\eta_2 = 10^{17}$ Pa s, $P_w = 400$ m and $L_a = 800$ m, respectively).

Depending on the viscosity of salt, the geometry of the diapir, and sedimentation rate most of the anhydrite layer is entrained in models where salt is assigned lower viscosity (Fig. 5). The variation in the viscosity of the salt effects the moulded geometry of the diapirs. However, as it is shown by Chemia et al. (2008) apart for the buried diapir, the height of the down-built diapirs where only the viscosity of the salt is varied evolves with negligible difference.

The stratigraphic location of the anhydrite layer controls the entrainment degree through salt supply. Variation in stratigraphy results in different salt supply (Fig. 8A). The model where the anhydrite layer is absent provides highest salt supply and variation in stratigraphy results in different entrainment rate (Fig. 8).

Model results show that the entrained anhydrite segments eventually sink within the diapir when salt supply decreases dramatically or ceases. In addition to the size and geometry of the entrained segments, viscosity of the salt is one of the main parameters that govern the rate of their descent. Anhydrite segments with relatively same size and geometry sink slower within the more viscous salt. Likewise, keeping viscosity constant, smaller segments sink slower.

7. Conclusions

Rate of salt supply in down-built diapirs is controlled by four parameters (sedimentation rate, viscosity of the salt, stratigraphy of the salt, and the perturbation width). It is illustrated here that these four parameters alter salt supply, which controls the shape of a down-build diapir. We conclude that salt supply controls the amount of entrainment and distribution of initially interbedded dense blocks/layers within a diapir, dictates the internal structure of the diapir.

Throughout the evolution of a diapir the amount of entrainment depends on salt supply to the diapir. With the range of parameters used in our models, entrainment of the anhydrite layer, which has been inevitable, was directly governed by the rate of salt supply. On the other hand, the entrained anhydrite segments sink within the diapir when salt supply decreases dramatically or ceases entirely. The rate of sinking at this stage depends strongly on the viscosity of the salt, anhydrite segments sink slower within more viscous salt.

Acknowledgements

We thank Christopher Talbot for comments on the manuscript and proof reading. The authors would like also to thank the anonymous reviewers for their valuable comments and the editor Robert E. Holdsworth for editorial comments. The Swedish Research Council (VR) provided funding.

References

Baar, C., 1977. Applied Salt Rock Mechanics 1: The In-Situ Behaviour of Salt Rocks. Developments in Geotechnical Engineering. Elsevier, Amsterdam, p. 249.
Bauerle, G., Bornemann, O., Mauthe, F., Michalzik, D., 2000. Origin of stylolites in Upper Premian zechstein anhydrite (Gorleben Salt Dome, Germany). Journal of Sedimentary Research 70 (3), 726–737.
Behlau, J., Mingerzahn, G., 2001. Geological and tectonic investigations in the former Morsleben salt mine (Germany) as a basis for the safety assessment of a radioactive waste repository. Engineering Geology 61 (2–3), 83–97.
Biot, M.A., 1965. Theory of viscous buckling and gravity instability of multilayers with large deformation. Geological Society of America Bulletin 76 (3), 371–378.
Carter, N.L., Horseman, S.T., Russell, J.E., Handin, J., 1993. Rheology of rocksalt. Journal of Structural Geology 15 (9–10), 1257–1271.
Chemia, Z., Koyi, H., Schmeling, H., 2008. Numerical modelling of rise and fall of a dense layer in salt diapirs. Geophysical Journal International 172 (2), 798–816.
Cruden, A.R., Koyi, H., Schmeling, H., 1995. Diapiric basal entrainment of mafic into felsic magma. Earth and Planetary Science Letters 131 (3–4), 321–340.

Gansser, A., 1992. The enigma of the Persian salt-dome inclusions. Eclogae Geologicae Helvetiae 85 (3), 825–846.
Heilbronner, R., Bruhn, D., 1998. The influence of three-dimensional grain size distributions on the rheology of polyphase rocks. Journal of Structural Geology 20 (6), 695–705.
Hudec, M.R., Jackson, M.P.A., 2007. Terra infirma: Understanding salt tectonics. Earth-Science Reviews 82 (1–2), 1–28.
Jackson, M.P.A., Talbot, C.J., 1986. External shapes, strain rates, and dynamics of salt structures. Geological Society of America Bulletin 97 (3), 305–323.
Jackson, M.P.A., Talbot, C.J., 1991. A glossary of salt tectonics. Bureau of Economic Geology, Geological Circular 91-4, Austin,Texas, p. 44.
Jackson, M.P.A., Vendeville, B.C., Schultz-Ela, D.D., 1994. Structural dynamics of salt systems. Annual Review of Earth and Planetary Sciences 22, 93–117.
Jenyon, M.K., 1986. Salt Tectonics. Elsevier Applied Science, London.
Kent, P.E., 1979. The emergent Hormuz salt plugs of southern Iran. Journal of Petroleum Geology 2, 117–144.
Kirby, S.H., Kronenberg, A.K., 1987. Rheology of the lithosphere: selected topics. Reviews of Geophysics 25 (6), 1219–1244.
Koyi, H.A., 1988. Experimental modeling of the role of gravity and lateral shortening in the Zagros mountain belt. AAPG Bulletin 72, 381–1394.
Koyi, H., 1998. The shaping of salt diapirs. Journal of Structural Geology 20 (4), 321–338.
Koyi, H., 2001. Modeling the influence of sinking anhydrite blocks on salt diapirs targeted for hazardous waste disposal. Geology 29 (5), 387–390.
Landolt-Boernstein, 1982. Numerical data and functional relationships in science and technology group, V: Geophysics and Space Research. Physical Propertes of Rocks 1a. Springer, New York, p. 373.
Poliakov, A.N.B., Van-Balen, R., Podladchikov, Y., Daudre, B., Cloetingh, S., Talbot, C., 1993. Numerical analysis of how sedimentation and redistribution of surficial sediments affects salt diapirism. Tectonophysics 226 (1–4), 199–216.
Ramberg, H., 1968. Instability of layered systems in the field of gravity. Physics of the Earth and Planetary Interiors 1 (7), 427–447.
Spiers, C.J., Schutjens, P.M.T.M., Brzesowsky, R.H., Peach, C.J., Liezenberg, J.L., Zwart, H.J., 1990. Experimental determination of constitutive parameters governing creep of rocksalt by pressure solution. In: Geological Society (Ed.), Deformation Mechanisms, Rheology and Tectonics. Geological Society special publication 54, London, pp. 215–227.
Talbot, C.J., 1995. Molding of salt diapirs by stiff overburden. In: Jackson, M.P.A., Roberts, D.G., Snelson, S. (Eds.), Salt Tectonics: A Global Perspective. AAPG Memoir, 65, pp. 61–75.
Urai, J.L., Spiers, C.J., Zwart, H.J., Lister, G.S., 1986. Weakening of rock salt by water during long-term creep (nuclear waste disposal). Nature 324 (6097), 554–557.
Van Berkel, J.T., Torrance, J.G., Schwerdtner, W.M., 1986. Deformed anhydrite nodules: A new type of finite strain gauge in sedimentary rocks. Tectonophysics 124 (3–4), 309–323.
Van Keken, P.E., Spiers, C.J., Van den Berg, A.P., Muyzert, E.J., 1993. The effective viscosity of rocksalt: implementation of steady-state creep laws in numerical models of salt diapirism. Tectonophysics 225 (4), 457–476.
Vendeville, B.C., Jackson, M.P.A., 1993. Rates of extension and deposition determine whether growth faults or salt diapirs form. In: Armentrout, J.M., Bloch, Roger, Olson, H.C., Perkins, B.F. (Eds.), Rates of Geologic Processes: Tectonics, Sedimentation, Eustasy and Climate: Implications for Hydrocarbon Exploration: Gulf Coast Section, Society of Economic Paleontologists and Mineralogists Foundation, fourteenth annual research conference, program with papers, pp. 263–268.
Vendeville, B.C., Jackson, M.P.A., Weijermars, R., 1993. Rates of salt flow in passive diapirs and their source layers. In: Armentrout, J.M., Bloch, Roger, Olson, H.C., Perkins, B.F. (Eds.), Rates of Geologic Processes: Tectonics, Sedimentation, Eustasy and Climate: Implications for Hydrocarbon Exploration: Gulf Coast Section, Society of Economic Paleontologists and Mineralogists Foundation, fourteenth annual research conference, program with papers, pp. 269–276.
Weinberg, R.F., 1993. The upward transport of inclusions in Newtonian and power-law salt diapirs. Tectonophysics 228 (3–4), 141–150.
Weinberg, R.F., Schmeling, H., 1992. Polydiapirs: multiwavelength gravity structures. Journal of Structural Geology 14 (4), 425–436.
Woidt, W.D., 1978. Finite element calculations applied to salt dome analysis. Tectonophysics 50, 369–386.
Zirngast, M., 1996. The development of the Gorleben salt dome (northwest Germany) based on quantitative analysis of peripheral sinks. Salt Tectonics. Special Publication 100. Geological Society, London. 203–226.